

- 950 (1989); G. A. Glatzmaier, G. Schubert, D. Berco-
vici, *Nature* **347**, 274 (1990).
29. For examples: Y. Ricard and W. Bai, *Geophys. J. Int.* **105**, 561 (1991); J. X. Mitrovica and A. M. Forte, *J. Geophys. Res.* **102**, 2751 (1997).
30. From the expressions for P and S wavespeed, $\alpha^2 = \kappa/\rho + 4/3 \mu/\rho$ and $\beta^2 = \mu/\rho$, respectively, one can obtain an expression for the bulk sound speed $\alpha^2 = \alpha^2 - 4/3 \beta^2 = \kappa/\rho$ and hence isolate the effects of the bulk (κ) and shear (μ) moduli (normalized by density). An important requirement for such joint inversions is that the P - and S -wave data are comparable in frequency content and sampling, and in particular the latter gives rise to complications at depths larger than 2000 km. [See G. S. Robertson and J. H. Woodhouse [*Earth Planet. Sci. Lett.* **143**, 197 (1996)], who studied the radial variation of $\nu = d \ln \beta / d \ln \alpha$ under the assumption of proportionality between P and S wavespeed.] Kennett *et al.* (32), therefore, selected short-period P - and S -wave data that sample along similar paths.
31. W.-j. Su and A. M. Dziewonski, *Phys. Earth Planet. Int.* **100**, 135 (1997).
32. B. L. N. Kennett, S. Widiyantoro, R. D. van der Hilst, *J. Geophys. Res.* **103**, 12469 (1998).
33. H. Bolton and G. Masters, *ibid.*, in press.
34. F. D. Stacey, *Phys. Earth Planet. Int.* **106**, 219 (1998).
35. R. A. W. Haddon and J. R. Cleary, *ibid.* **8**, 211 (1974); M. Hedlin, P. Shearer, P. S. Earle, *Nature* **387**, 145 (1997); P. M. Shearer, M. A. H. Hedlin, P. S. Earle, in (24), pp. 37–56. Caveat: Scatterers in the bottom 1000 km of the mantle produce precursors to the PKP phase arrival; scatterers at shallower depth cannot be excluded, but they produce arrivals in the coda of PKP that are more difficult to analyze.
36. S. Kaneshima and G. Helffrich, *J. Geophys. Res.* **103**, 4825 (1998).
37. J. Ritsema, S. Ni, D. V. Helmberger, and H. P. Crotwell [*Geophys. Res. Lett.* **25**, 4245 (1998)] concluded that beneath Africa a profound shear-wavespeed anomaly (with $\delta\beta/\beta$ 3% lower than average) extends up to 1500 km above the CMB.
38. P. J. Tackley, in (24), pp. 231–254.
39. Depending on how anelasticity is accounted for, D. A. Yuen *et al.* [in *Seismic Modeling of Earth Structure*, E. Boschi, G. Ekström, A. Morelli, Eds. (Istituto Nazionale di Geofisica, Rome, 1996), pp. 463–505] argue that the excess temperature required to produce a 3 to 5% shear-wavespeed perturbation is 1000 to 2600 K. T. J. Ahrens [*Eos* (fall suppl.) **79**, F846 (1998)] and Q. Williams [in (24), pp. 73–82] estimate that the temperature drop across the thermal boundary is 400 to 1400 K or 1000 to 2000 K, respectively.
40. At the CMB, thermal instabilities are formed when temperature contrasts ΔT exceed 300 K, which is of the same magnitude as excess temperatures of thermal plumes. Intrinsically dense material (i) reduces the seismic wavespeeds and the thermal anomaly required to explain them and (ii) gravitationally stabilizes the layer so that a larger ΔT can be supported [N. Sleep, *Geophys. J. R. Astron. Soc.* **95**, 437 (1988); C. Farnetani, *Geophys. Res. Lett.* **24**, 1583 (1997); R. Jeanloz and Q. Williams, *Rev. Mineral.* **37**, 241 (1998)].
41. M. J. Brown and T. J. Shankland, *Geophys. J. R. Astron. Soc.* **66**, 579 (1981)
42. F. D. Stacey, *Phys. Earth Planet. Int.* **99**, 189 (1997).
43. The solidus and adiabatic temperature gradients diverge in the lower mantle [A. Zerr, A. Diegeler, R. Boehler, *Science* **281**, 243 (1998)]. Viscosity depends on homologous temperature— $\eta(T) \propto \exp(30T_m/T)$ —and increases more than expected from geodynamic data if the temperature gradient is close to adiabatic [T. Spohn and G. Schubert, *J. Geophys. Res.* **87**, 4682 (1982)]. This argument depends on the choice of either the melting or solidus temperature for T_m , and neither is very well constrained for lower-mantle P - T conditions, but formulations based on activation volume and energy also predict a lower-mantle viscosity that is too high. Recent studies do argue for a large viscosity increase with depth, perhaps reaching a maximum at ~ 2000 km (29, 45), but the results are nonunique and the increase is still smaller than expected for an adiabatic geotherm.
44. B. L. N. Kennett [*Geophys. J. Int.* **132**, 374 (1998)]; *Eos* (fall suppl.) **79**, F599 (1998)] argues that in the deep mantle dp/dz is smaller than in PREM [A. M. Dziewonski and D. L. Anderson, *Phys. Earth Planet. Int.* **25**, 297 (1981)], in which it is close to adiabatic.
45. P. E. van Keken, D. A. Yuen, A. P. van den Berg, *Science* **264**, 1437 (1994); A. P. van den Berg and D. A. Yuen, *Phys. Earth Planet. Int.* **108**, 219 (1998).
46. (i) There is a strong dependence on the reference Earth model chosen for such analyses, as shown by T. J. Shankland and M. J. Brown [*Phys. Earth Planet. Int.* **38**, 51 (1985)]. Low-order polynomials used for the parameterization of reference models such as PREM [in (44)] may smooth variations over relatively short depth intervals; a flexible parameterization is required to constrain subtle deviations from adiabaticity (34, 44). (ii) The use of either the dynamic or static moment of inertia in density calculations affects the inferred density gradient (44). (iii) In general, propagation speed is better determined by seismic imaging than density variations. This poses a difficulty in fitting finite-strain equations of state to seismological models of the lower mantle, because density and its zero pressure value are required (34). (iv) Owing to bulk attenuation and the time scale on which internal stresses are relaxed, there is a subtle but important difference between the bulk modulus as deduced from seismic-wave propagation and the bulk modulus for a dynamic Earth that should be used in the Adams-Williams equation that underlies the definition of the inhomogeneity parameter [D. L. Heinz, R. Jeanloz, R. J. O'Connell, *J. Geophys. Res.* **87**, 7772 (1982); D. L. Heinz and R. Jeanloz, *Nature* **301**, 138 (1983); (42)]. In addition, multiphase systems should be considered in analyses of bulk attenuation (34). (v) The concept of adiabaticity is valid for compositionally homogeneous media only; in the case of a chemical stratification the temperature may seem "superadiabatic" although radial variations in density may be similar to those expected from adiabatic compression.
47. G. F. Davies, *J. Geophys. Res.* **89**, 6017 (1984); M. Gurnis, *Geophys. Res. Lett.* **13**, 1474 (1986); M. Manga, *ibid.* **23**, 403 (1996).
48. U. Hansen and D. A. Yuen, *Nature* **334**, 237 (1988); *Geophys. Res. Lett.* **16**, 629 (1988).
49. J. Tromp and M. Ishii, *Eos* (fall suppl.) **79**, F598 (1998).
50. G. Serghiou, A. Zerr, R. Boehler, *Science* **280**, 2093 (1998).
51. C. Meade, H.-k. Mao, J. Hu, *ibid.* **268**, 1743 (1995); S. Saxena *et al.*, *ibid.* **274**, 1357 (1995).
52. L. Stixrude and M. S. T. Bukowski, *J. Geophys. Res.* **95**, 19311 (1990); L. Dubrovinsky *et al.*, *Geophys. Res. Lett.* **25**, 4253 (1998).
53. Y. Tsuchida and T. Yagi, *Nature* **340**, 217 (1989); K. J. Kingma *et al.*, *ibid.* **374**, 243 (1995); L. S. Dubrovinsky *et al.*, *ibid.* **388**, 363 (1997).
54. H.-k. Mao, G. Shen, R. J. Hemley, *Science* **278**, 2098 (1997); L. Stixrude, in (24), pp. 83–96.
55. D. L. Anderson, in (24), pp. 255–272.
56. At $P > 70$ to 90 GPa, FeO can transform to NiAs structure with $\delta\rho/\rho > 4\%$; the transition has a negative Clapeyron slope and is thus more likely to occur at high temperatures [R. Jeanloz and T. H. Ahrens, *Geophys. J. R. Astron. Soc.* **62**, 505 (1980); H.-k. Mao, J. Shu, Y. Fei, J. Hu, R. J. Hemley, *Phys. Earth Planet. Int.* **96**, 135 (1996)].
57. On the basis of the dihedral angle of melts (slightly larger than optimal percolation but much smaller than for upper-mantle conditions), M. C. Shannon and C. B. Agee [*Science* **280**, 1059 (1998)] argued that under lower-mantle conditions, efficient percolation of iron is possible in perovskite—perhaps not, however, in magnesiowüstite (C. B. Agee, personal communication).
58. We thank the participants of the 1998 MIT-WHOI-Harvard joint course on "Mantle Convection" and P. Bunge, A. Forte, S. Grand, F. Guyot, S. Karato, B. Kennett, L. Kellogg, J.-P. Montagner, S. Saxena, and J. Trampert for stimulating discussions. We thank C. Bina and B. Kennett for valuable comments on earlier versions of the manuscript. Two anonymous referees provided constructive reviews. R.v.d.H. gratefully acknowledges the Institut de Physique du Globe de Paris, France, for the hospitality during his visit when most of this report was written. S. Zhong and F. Simons produced Fig. 3. Funded under NSF grant EAR96-28087.

9 November 1998; accepted 3 February 1999

Dipping Low-Velocity Layer in the Mid-Lower Mantle: Evidence for Geochemical Heterogeneity

Satoshi Kaneshima^{1*} and George Helffrich²

Data from western United States short-period seismic networks reveal a conversion from an S to a P wave within a low seismic velocity layer (greater than or equal to the 4 percent velocity difference compared to the surrounding mantle) in the mid-lower mantle (1400 to 1600 kilometers deep) east of the Mariana and Izu-Bonin subduction zones. The low-velocity layer (about 8 kilometers thick) dips 30° to 40° southward and is at least 500 kilometers by 300 kilometers. Its steep dip, large velocity contrast, and sharpness imply a chemical rather than a thermal origin. Ancient oceanic crust subducted into the lower mantle is a plausible candidate for the low-velocity layer because of its broad thin extent.

Planetary differentiation and convection create heterogeneities in the mantle, which are ultimately related to the cooling of Earth over the age of the solar system. Seismically, these

heterogeneities express themselves in velocity heterogeneity due to variations in temperature, bulk composition, and phase changes in the mantle. In the upper mantle, all three mechanisms act, accounting for the greater velocity variations there ($\pm 5\%$) in comparison to the lower mantle ($\pm 0.5\%$) (1). In the lower mantle, it is not clear which mechanisms act, because the lower mantle seems comparatively homogeneous except for the

¹Department of Earth and Planetary Sciences, Faculty of Science, Tokyo Institute of Technology, Ookayama, Meguro-ku, Tokyo 152, Japan. ²Department of Geology, University of Bristol, Queens Road, Bristol, UK.

*To whom correspondence should be addressed.

lowermost 200 to 300 km of the mantle (D'') and upper mantle slab extensions (2). We used a seismic array-based technique to find what are likely to be the more subtle lower mantle heterogeneities, which should provide information on Earth's longer term evolution.

Evidence for seismic velocity anomalies smaller than 500 km comes from the discrepancy between shear-wave velocities, which were derived from body waves and normal mode studies (3), and from a recent study of global stacking of core phase PKP precursors (4), yielding statistical models of heterogeneity in the mantle but not their individual positions. We refined the size, shape, and velocity contrast of one previously recognized heterogeneity in the mid-lower mantle (5) by analyzing later arrivals after P waves from intermediate to deep focus earthquakes at the Mariana trench to the south of the Izu-Bonin trench (Fig. 1).

The data are short-period seismograms from western United States networks for intermediate (~200 km) to deep (~600 km) earthquakes that occurred from 1993 to 1996. The later arrival (indicated by arrows in Fig. 2 and called "later phase" hereafter) for these events shows a systematic focal depth-delay time trend (Table 1). This result indicates that the later phase was caused by the conversion of an S wave to a P wave at a mid-lower mantle velocity heterogeneity (5). We located the source of the later phase for the five events on the basis of maximizing the scattering likelihood, which was computed with the observed travel time δt , slowness δp , and arrival azimuth $\delta\phi$ in relation to direct P waves (Table 1) (6). The conversion points, or scatterers, form a plane (500 km by 300 km) dipping ~30° southward (Fig. 1, inset, and Table 1). The plane's dip angle is consistent with dips that were independently determined, assuming that Snell's law holds at the wave conversion point across the interface (Fig. 1, inset) (5). We conclude from this mapping that the lower mantle heterogeneity is a nearly planar interface extending at least several hundred kilometers and that the later phases are the S-to-P converted waves at this dipping interface (Fig. 3A).

The stacked later phase waveforms differ slightly from the direct P waveform stacks.

To model the interface's properties, we compared synthetic waveforms with the stacked waveforms of the later phase (7) (Fig. 3B). Two classes of interface models in which elastic property discontinuously changes across planar boundaries can explain the waveforms (Fig. 3A). The first has a $\geq 8\%$ velocity increase from above the interface to below (5). The other has a thin ~8-km-thick layer of $\geq 4\%$ lower velocity than the surrounding mantle. This thin low-velocity layer model gives systematically larger correlation values by 0.05 to 0.1 than the first model for almost all array-event pairs (Fig. 3C). The synthetic waveforms for the second model yield the subtle but characteristic downsloping onset of the later phase, which is not produced by the first model (Fig. 3B, arrows). On this account, we favor the second, thin low-velocity layer model for the source of

S-to-P converted waves in the mid-lower mantle, which also requires a velocity heterogeneity that is half that of the first model (8).

The relative amplitudes of the later phase to direct P waves depend on its frequency content. At higher frequencies, amplitudes fall off above 0.25 Hz, whereas at lower frequencies, they fall off below 0.15 Hz (5). The lower frequency falloff is qualitatively consistent with the model of a layer that is not thick in comparison to the wavelength of incoming waves (5 to 10 km). The estimated velocity anomaly has a large uncertainty (at least a factor of 2) because of the factors that influence the observed amplitude ratios. These factors include the attenuation structure of the mantle between the foci and the conversion points and the relative radiation intensity of the S wave to the direct P wave, resulting from uncertainties in the focal

Fig. 1. Map of the study area, showing earthquakes, S-to-P wave conversion points, and present and past trench locations. Open diamonds indicate earthquake epicenters (Table 1). Thick solid lines represent the present trench lines, and broken lines indicate the reconstructed locations of the Indonesia trench during the Mesozoic era (13). The trench migrated southwestward during the Mesozoic era. Solid squares denote the S-to-P wave conversion point locations. The ray paths projected onto the horizontal plane of a direct P wave and of an S-to-P converted wave are shown with thin solid lines. (Inset) A cross section of the S-to-P wave conversion points along section A-B. Solid squares show the locations of the conversion points, and solid bars represent dip angles of the conversion interfaces, which were determined by applying Snell's law to the rays of incoming S waves and converted P waves.

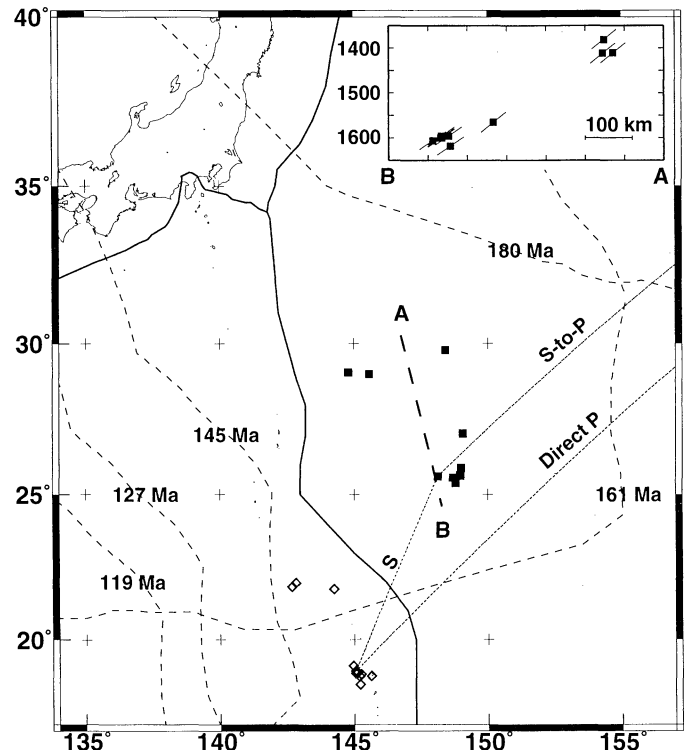


Table 1. Event list and conversion point locations. Lat., latitude; Long., longitude; deg., degree; mb, body-wave magnitude.

Event	Date	Time, UT	Lat., °N	Long., °E	Depth, km	mb	δt , s	δp , s/deg.	$\delta\phi$, deg.	Lat., °N	Long., °E	Depth, km	Likelihood
1	4/2/93	1432:19	18.42	145.22	501	5.2	100.7	-0.20	3.0	25.90 ± 0.12	148.99 ± 0.18	1618 ± 8	0.95 ± 0.01
2	7/22/93	1215:36	21.76	144.26	127	5.6	123.0	-0.10	3.5	29.79 ± 0.06	148.42 ± 0.20	1381 ± 6	0.84 ± 0.01
3	4/8/95	1745:13	21.83	142.69	267	6.4	107.7	-0.20	4.0	29.06 ± 0.10	144.79 ± 0.22	1411 ± 7	0.95 ± 0.03
4	7/6/96	2136:29	21.97	142.83	241	5.8	110.0	-0.20	3.5	29.00 ± 0.12	145.57 ± 0.21	1412 ± 8	0.95 ± 0.02
5	7/15/96	1651:22	18.73	145.63	177	5.9	129.0	-0.25	4.0	27.05 ± 0.13	149.06 ± 0.22	1565 ± 7	0.95 ± 0.03
6*	8/24/95	0155:35	18.90	145.05	588	6.0	88.6	-0.20	3.0	25.62 ± 0.08	148.13 ± 0.23	1596 ± 5	0.95 ± 0.02

*Representative hypocenter, conversion point location, and δt , δp , and $\delta\phi$ for the previously analyzed August 1995 earthquake sequence (5). The conversion points of all of the events of the sequence are clustered within a small region (Fig. 1).

mechanisms of the earthquakes (9). The shear velocity anomaly of 4% is a lower bound when we use lower attenuation and higher estimates of *S*-wave radiation intensity (see the caption of Fig. 3B). If we adopt the preliminary reference Earth model's (PREM's) attenuation model (10) or small estimates of the radiation intensity or both, the amount of the velocity anomaly can exceed 8%.

The geometry and properties of the heterogeneity constrain possibilities for its origin. A shear velocity heterogeneity (at least 4% slower than the surrounding mantle) that is this sharp probably cannot be solely due to temperature, because a high-temperature anomaly exceeding 500 K is required and the diffusive time scale for heat loss τ for a 8-km-thick slab is only 2 million years (My) ($\tau = L^2/D$ and $D \approx 10^{-6} \text{ m}^2 \text{ s}^{-1}$, where L and D are the layer thickness and thermal diffusivity, respectively). The dipping feature of the object rejects a pressure-driven phase transition (11). Thus, it represents a chemically distinct region even if a thermal anomaly is also present. The heterogeneity's shape and thickness suggest oceanic crust that was subducted into the lower mantle, with its different bulk composition expressed as the velocity contrast with the surrounding mantle. We assess the plausibility of the model in the following. Slabs subducted during the Cenozoic era do not have any relation with this heterogeneity (12) nor do recent tomographic models reveal velocity anomalies in this region (2). On the other hand, a reconstruction of paleosubduction zones indicates that the Indonesia slab was located above the heterogeneity with an age of 160 to 170 million years ago (Fig. 1) (13). Velocities in plausible subducted basaltic mineral assemblages in the mid-lower mantle vary by only $\sim 1.5\%$ in relation to pyrolite (14), but the shear modulus behavior at lower mantle conditions is too uncertain to exclude a contrast with subducted basalt. It is therefore uncertain at this stage if the observed velocity heterogeneity represents subducted oceanic crust, but other Earth structures with this thickness and lateral extent are difficult to envisage.

If the detected heterogeneity represents the oceanic crustal part of a Mesozoic slab, several consequences for mantle dynamics and geochemistry follow. The heterogeneity's residence time in the mantle is of the order of 160 My. Its planar shape indicates that buckling or folding of slabs is insignificant at scales smaller than 500 km. The dip of the observed layer is opposite to the northward dipping subduction of the Indonesia slab predicted from plate reconstructions (13), which may indicate that the slab lay horizontally stagnant above the 660-km discontinuity before descending into the lower

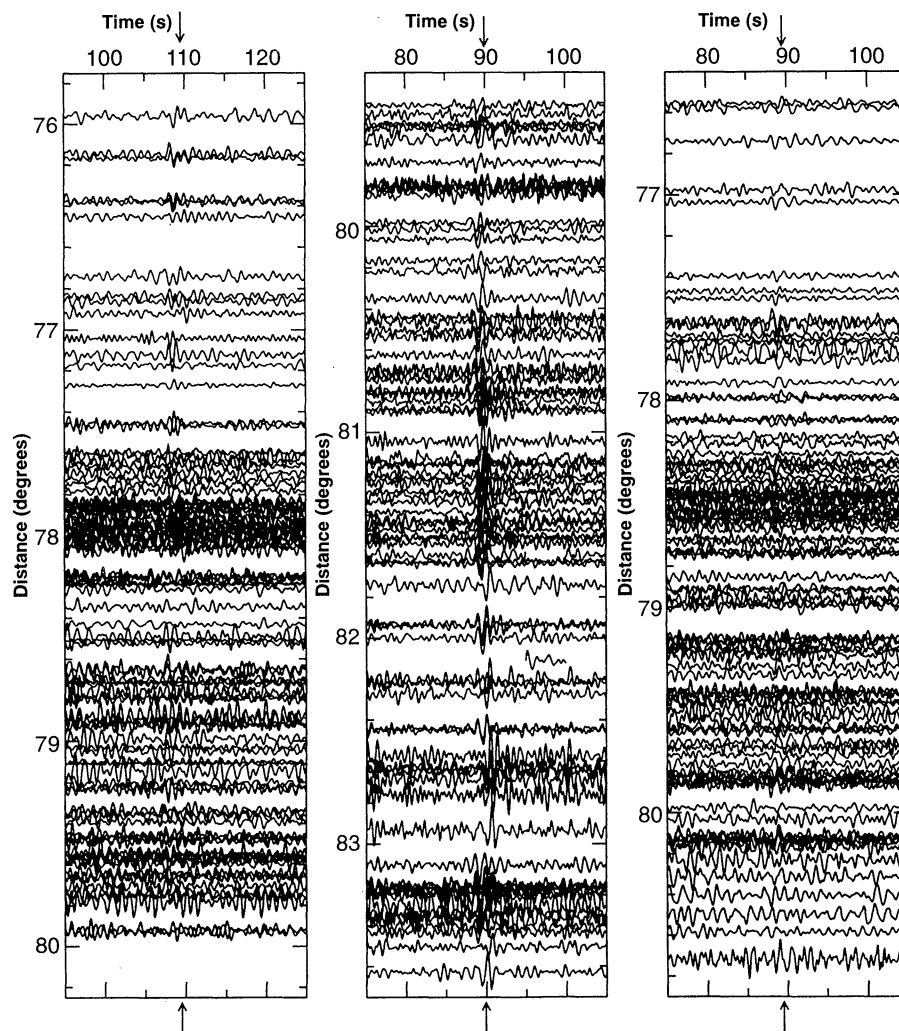


Fig. 2. Record sections of the vertical components of short-period seismograms. Seismograms are bandpass filtered from 0.2 to 2 Hz. The horizontal axes are the delay times (in seconds) after the onsets of direct *P* waves. The vertical axes are the epicentral distances in degrees. Event 3 in Table 1, recorded at the University of Washington Network (left). Event 6 in Table 1 (24 August 1995, 0628 UT), recorded at the Northern California Earthquake Center Network (middle). Event 6 in Table 1 (24 August 1995, 0155 UT), recorded at the University of Washington Network (right). The isolated and impulsive phases denoted by arrows (not predicted by any standard Earth models) are the later phases we studied.

mantle (15). The near absence of western Pacific hot spots (16) might also be a consequence of the same phenomenon if their rise from the lower mantle is found to be blocked by stagnant slabs such as this one. If the characteristic plume rise time was 15 to 30 My (17) and the slab remained there for at least 160 My, it would effectively screen hot spot rising and may become entrained in plume ascent, a feature entailed in some geochemical models (18).

The reservoir dimensions suggested by these observations constrain some models of lower mantle geochemical heterogeneity as well. A sheet of subducted oceanic crust can deliver the ^{238}U that is required for the mantle's high μ (HIMU) ($\mu = ^{238}\text{U}/^{204}\text{Pb}$) component. Uranium decay produces ^4He , which if sequestered in an ~ 8 -km-thick

layer, would be nearly closed to He diffusion for the ≥ 1 -billion-year time scale required to generate the observed $^{207/204}\text{Pb}-^{206/204}\text{Pb}$ arrays in mid-ocean ridge basalt (MORB) and oceanic island basalt (OIB) (19, 20). Consequently, if these objects were to be sampled during OIB genesis, say by plumes, they would link a low $^3\text{He}/^4\text{He}$ component to HIMU. However, the generally 5 to 7 R_A (R_A , atmospheric ratio) $^3\text{He}/^4\text{He}$ ratios of HIMU OIBs suggest segregation times of ~ 100 My (19), which are shorter than the ~ 160 -My residence time of the objects estimated above. One way to break the link between HIMU and low $^3\text{He}/^4\text{He}$ is to postulate the diffusive loss of He out of a thin HIMU source body that is 0.2 to 3 km thick (19), thinner than the sheet we observe. Alternatively, a thicker

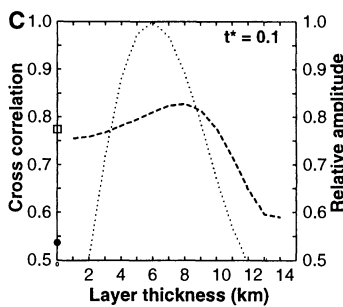
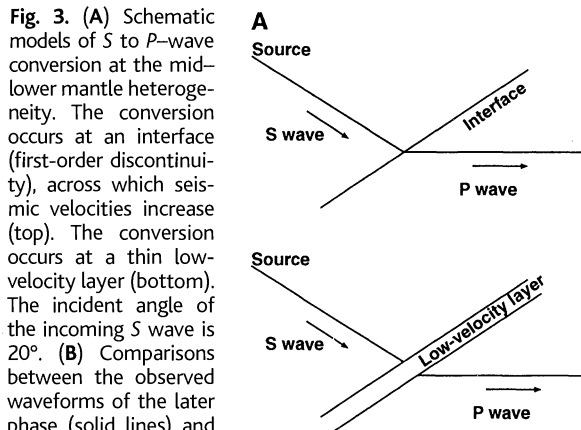
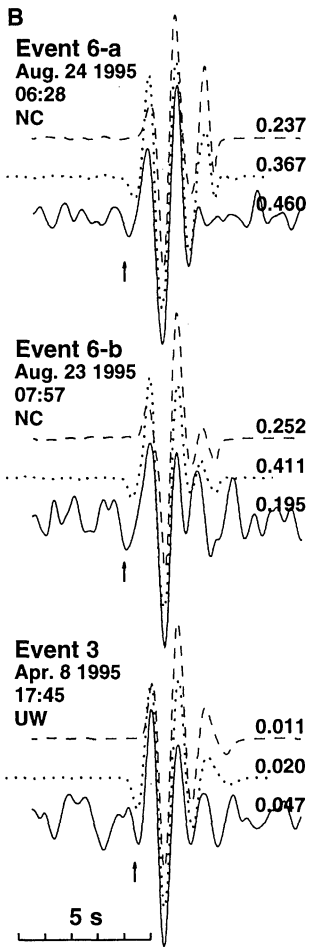


Fig. 3. (A) Schematic models of *S* to *P*-wave conversion at the mid-lower mantle heterogeneity. The conversion occurs at an interface (first-order discontinuity), across which seismic velocities increase (top). The conversion occurs at a thin low-velocity layer (bottom). The incident angle of the incoming *S* wave is 20°. (B) Comparisons between the observed waveforms of the later phase (solid lines) and synthetics (22). These examples show the cases recorded at the Northern California array (NC) or at the University of Washington array (UW) (5) (event 3 and two events included in event 6, Table 1). Broken lines indicate a 4% velocity increase across a single interface; dotted lines indicate a 4% low-velocity layer that is 8 km thick. Numbers at the right of the linearly stacked waveforms are the amplitudes of the later phase in relation to direct *P*. Arrows indicate the downswing onsets of the later phases. Radiation intensities were computed on the basis of the Harvard Centroid Moment Tensor solutions, allowing a 5° uncertainty of the nodal planes and taking the maximum possible values (9), which can be nearly four times larger than the minimum values. Waveforms of the deeper and shallower events are both consistent with the low-velocity thin-layer model. (C) Cross correlation between the observed and synthetic waveforms with normalized amplitudes of synthetic waveforms averaged over deep events. Broken line indicates cross correlations as a function of layer thickness for a low-velocity thin-layer model. Cross correlation reaches a maximum at a thickness of 8 km, and the maximum for the velocity increase at a single interface is shown with a open square at a layer thickness of 0 km. The dotted line indicates the amplitudes of the *S*-to-*P* converted waves, which were normalized to the maximum that was obtained for a thickness of 6 to 7 km. The closed circle at a thickness of 0 km represents the relative amplitude for the single-interface model and t^* represents the value of δt^* defined in (22).



body would require a lower internal $^3\text{He}/^4\text{He}$ ratio and mixing with the MORB reservoir to attain the observed HIMU OIB ratio. If the sheet is a relatively new feature in the mantle, whose shape will be disrupted by future stirring, the diffusive model may be compatible with the sheet's thickness. However, the strong elastic contrast may plausibly be linked to an equally strong rheological contrast, which would inhibit further mixing. Thus, geochemical heterogeneity longevity may be longer than envisaged in mixing simulations in viscously homogeneous fluids (20, 21).

References and Notes

1. A. M. Dziewonski, *J. Geophys. Res.* **89**, 5929 (1984).
 2. T. Sakurai, thesis, University of Tokyo (1996); R. D. van der Hilst, S. Widiyantoro, E. R. Engdahl, *Nature* **386**, 578 (1997); S. P. Grand, R. D. van der Hilst, S. Widiyantoro, *GSA Today* **7**, 1 (1997).

3. G. Nolet and T.-J. Moser, *Geophys. J. Int.* **114**, 185 (1993).
 4. M. Hedlin, P. M. Shearer, P. S. Earle, *Nature* **387**, 145 (1997).
 5. S. Kaneshima and G. Helffrich, *J. Geophys. Res.* **103**, 4825 (1998).
 6. We define the scattering likelihood of each point as $\exp[-(\delta\rho - \delta\rho_c)^2/\varepsilon_\rho^2 - (\delta\phi - \delta\phi_c)^2/\varepsilon_\phi^2 - (\delta t - \delta t_c)^2/\varepsilon_t^2]$, where $\delta\rho_c$, $\delta\phi_c$, δt_c are slowness, back azimuth, and travel time, respectively, predicted from single scattering at that point. The uncertainties of each variable are ε_ρ , ε_ϕ , and ε_t , respectively. The errors in the horizontal and vertical locations are estimated as nearly 20 and 8 km, respectively (Table 1).
 7. We assumed the geometrical ray theory and computed waveforms of the *S*-to-*P* converted wave at plane interfaces. Three-dimensional ray tracing was performed for *S*-to-*P* converted waves at interfaces embedded in a radially stratified Earth model. The frequency-dependent phase shift at conversion was modeled in the Thomson-Haskell propagator matrix approach [K. Aki and P. G. Richards, *Quantitative Seismology: Theory and Methods* (Freeman, New York, 1980)], and a filter representing waveform distortions due to causal attenuation

was convolved. Application of the geometrical ray theory should suffice for computing waveforms except at rather limited critical points such as caustics [C. H. Chapman, *J. Geophys.* **58**, 27 (1985)], which was not the case in this study.
 8. Two further relevant observations are (i) the waveform data of event 6 recorded at the UK short-period seismometer array, which is located at a different source-receiver azimuth (345°) from the western U.S. arrays (55°), show no substantial signals around the times corresponding to the mid-lower mantle *S*-to-*P* scattering waves and (ii) a semblance technique that computes single scattering likelihood applied to the global broadband network data shows that large signals corresponding to the mid-lower mantle *S*-to-*P* waves are visible only at those along azimuths to North America. These indicate that the energy radiated by the *S*-to-*P* conversion is along a limited azimuth. This is consistent with either an *S*-to-*P* conversion at dipping flat interfaces or angle-dependent point scattering.
 9. G. R. Helffrich, *Geophys. J. Int.* **131**, 741 (1998).
 10. A. M. Dziewonski and D. L. Anderson, *Phys. Earth Planet. Inter.* **25**, 297 (1981).
 11. Array analyses of short-period or broadband waveforms have resulted in reports of several lower mantle seismic discontinuities [H. Kawakatsu and F. Niu, *Nature* **371**, 301 (1994); Y. Le Stunff, C. W. Wicks Jr., B. Romanowicz, *Science* **270**, 74 (1995)], but the presence of a steep dip of discontinuity has not been confirmed.
 12. We assumed on the basis of field data from Japan [R. E. van der Hilst and T. Seno, *Earth. Planet. Sci. Lett.* **120**, 395 (1993)], that the Philippine plate-Pacific plate-Eurasia plate triple junction migrated eastward to its present position south of Izu peninsula, near Tokyo. This migration puts subduction farther west than the present Izu-Bonin and Mariana trenches. Also, dip and strike of the sheet argue against a Cenozoic Izu-Bonin subduction origin and indicate that the subduction origin is older than the Cenozoic.
 13. D. C. Engebretson, A. Cox, R. G. Gordon, *Geol. Soc. Am. Spec. Pap.* **206**, 59 (1985).
 14. Mineral assemblages of subducted basalt in the mid-lower mantle are assumed to be made up of ~20% Ca-perovskite, 3 to 20% stishovite, and 60 to 77% Mg-Fe-perovskite by volume with molar Mg/(Mg + Fe) of 0.60 to 0.70, whereas those of pyrolyte are made up of 6% Ca-perovskite, 74% Mg-Fe-perovskite, and 20% magnesio-wüstite.
 15. J. B. Gaherty and B. H. Hager, *Geophys. Res. Lett.* **21**, 141 (1994).
 16. P. R. Vogt, *J. Geophys. Res.* **86**, 950 (1981).
 17. M. A. Richards, R. A. Duncan, V. E. Courtillot, *Science* **246**, 103 (1989).
 18. A. W. Hofmann, *Nature* **385**, 219 (1997).
 19. T. Hanyu and I. Kaneoka, *ibid.* **390**, 273 (1997).
 20. U. R. Christensen and A. W. Hofmann, *J. Geophys. Res.* **99**, 19867 (1994).
 21. G. F. Davies and M. A. Richards, *J. Geol.* **100**, 151 (1992); L. H. Kellogg, *Annu. Rev. Earth Planet. Sci.* **20**, 365 (1992).
 22. Comparing synthetics with linearly stacked array waveforms whose relative slownesses and back-azimuth deviations maximize the beam strength, we assumed a differential attenuation δt^* ($t^* = t/Q$, where t and Q are travel time and quality factor, respectively) of 0.1 for deep events (~600 km) on the basis of a depth-dependent absorption band model [D. L. Anderson and J. W. Given, *J. Geophys. Res.* **87**, 3893 (1982)]. For shallower events (~250 km), δt^* of 0.2 is used.
 23. We thank the two anonymous reviewers for useful comments and owe a debt of gratitude to the Incorporated Research Institutions for Seismology Data Management Center, the University of Washington, the Northern California Earthquake Center, and the British Geological Survey, who supplied waveform data.

29 October 1998; accepted 8 February 1999